Electronic Supplementary Material (ESI) for Journal of Materials Chemistry A.

Supporting information

Defects lead to a massive enhancement in UV-Vis-IR driven thermocatalytic activity of Co_3O_4 mesoporous nanorods

Lan Lan, Zhengkang Shi, Qian Zhang, Yuanzhi Li, Yi Yang, Shaowen Wu, Xiujian Zhao*

State Key Laboratory of Silicate Materials for Architectures (Wuhan University of Technology), 122 Luoshi Road, Wuhan 430070, P. R. China. Email: liyuanzhi66@hotmail.com

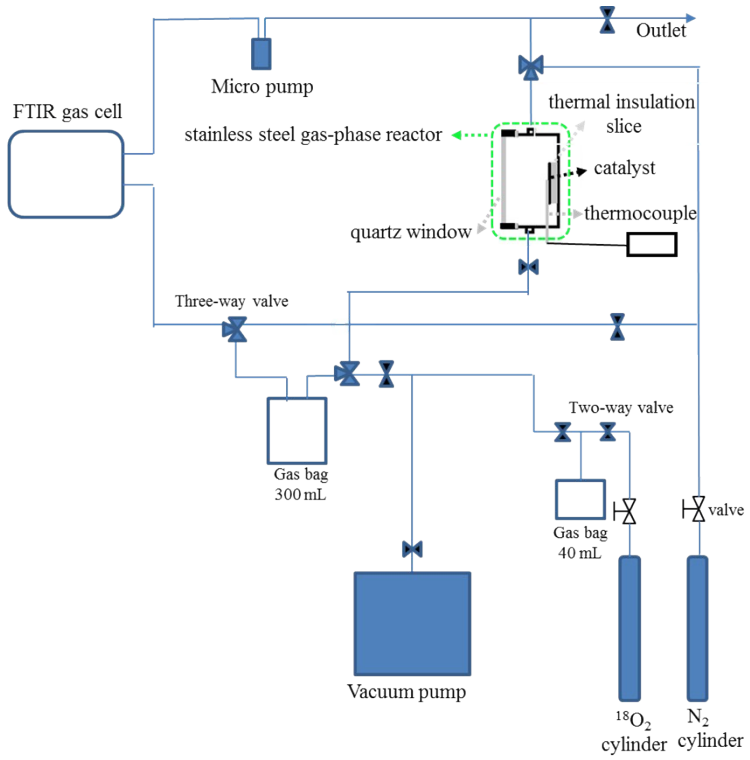

Scheme S1. The Set-up of isotope labeling experiment for the oxidation of benzene ($^{12}C_6{}^1H_6$) by $^{18}O_2$ on the Co_3O_4-MNR sample under the illumination from the Xe lamp.

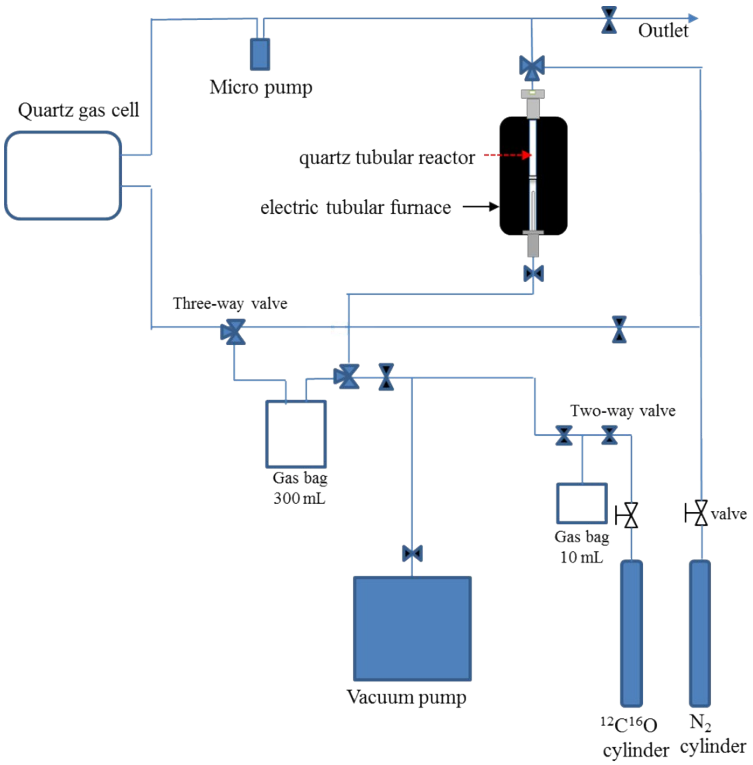

Scheme S2. The set-up for heating the used Co_3O_4-MNR sample (after the $^{18}O_2$ isotope experiment) in an atmosphere of $^{12}C^{16}O$ and N_2 at a known heating rate.

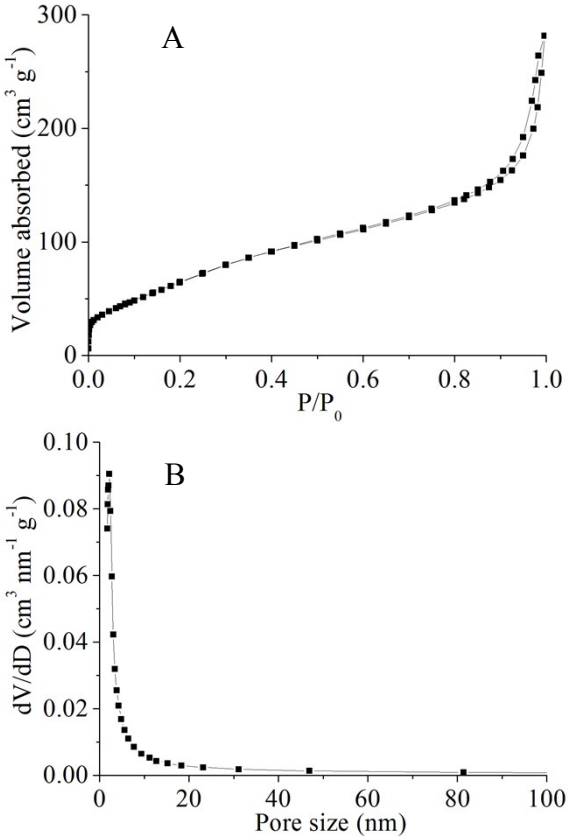

Figure S1. N_2 adsorption–desorption isotherm (A) and pore size distribution (B) of Co_3O_4-MNR.

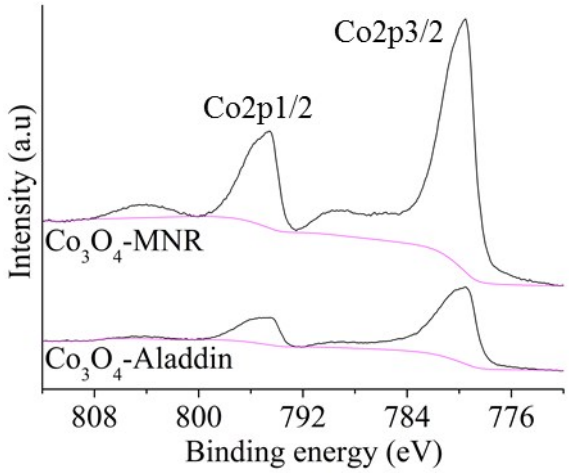

Figure S2. The XPS spectra of Co2p of the samples.

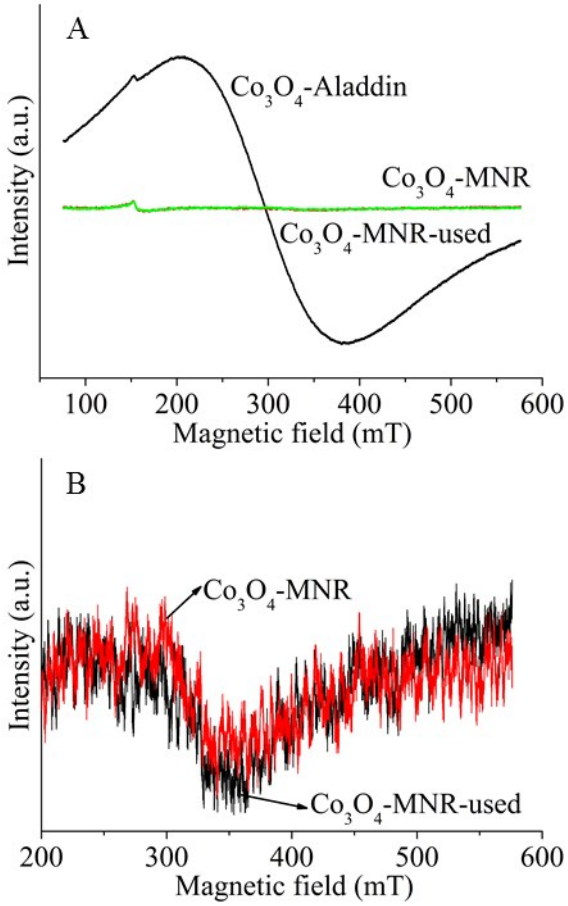

Figure S3. The EPR spectra of Co_3O_4-MNR, Co_3O_4-Aladdin, and the used Co_3O_4-MNR sample after the photothermocatalytic durability tests (A). The EPR spectra (enlarged from Figure S3A) of Co_3O_4-MNR and the used Co_3O_4-MNR sample after the photothermocatalytic durability tests (B): The values of *g* for Co_3O_4-Aladdin, Co_3O_4-MNR, and the used Co_3O_4-MNR sample after the photothermocatalytic durability tests are 2.185, 2.033, and 2.033 respectively.

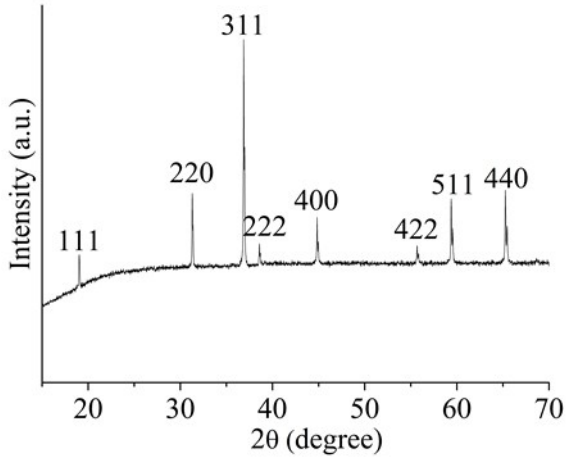

Figure S4. XRD patterns of the Co_3O_4-Aladdin sample.

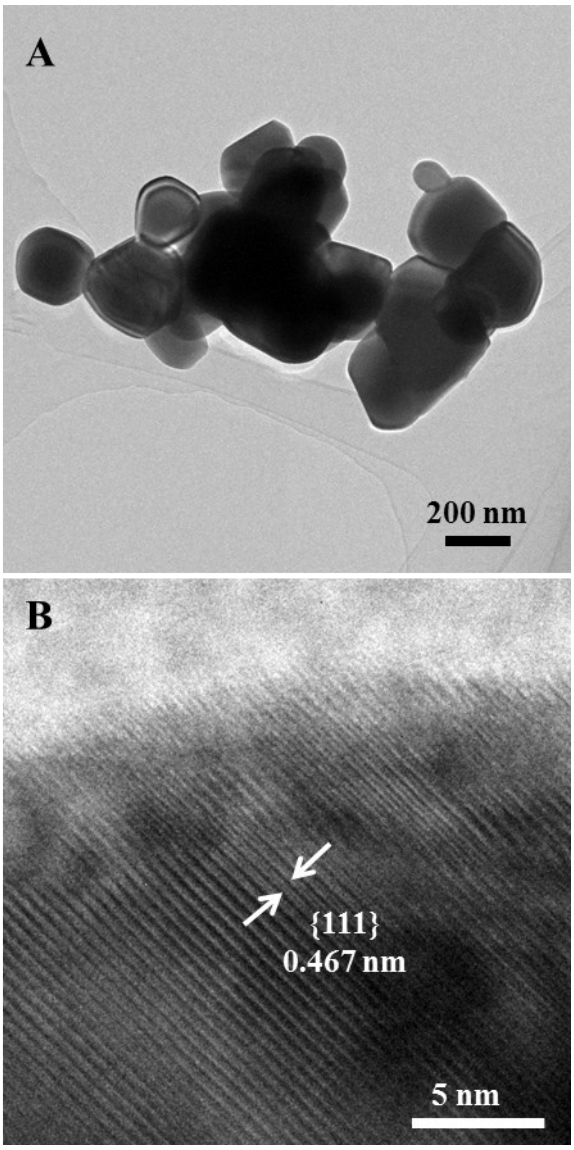

Figure S5. TEM (A) and HRTEM (B) images of the commercial Co_3O_4-Aladdin sample.

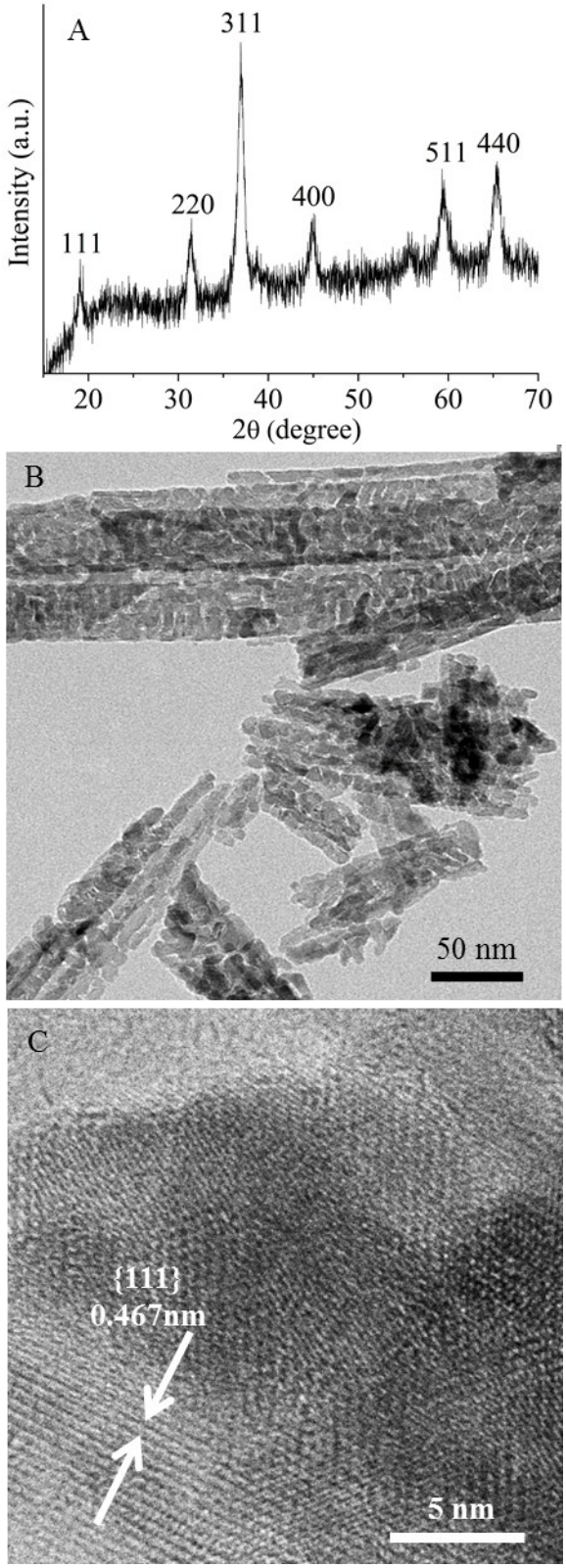

Figure S6. The XRD patterns (A), TEM (B), and HRTEM (C) of the used Co_3O_4-MNR sample after the photothermocatalytic durability tests.

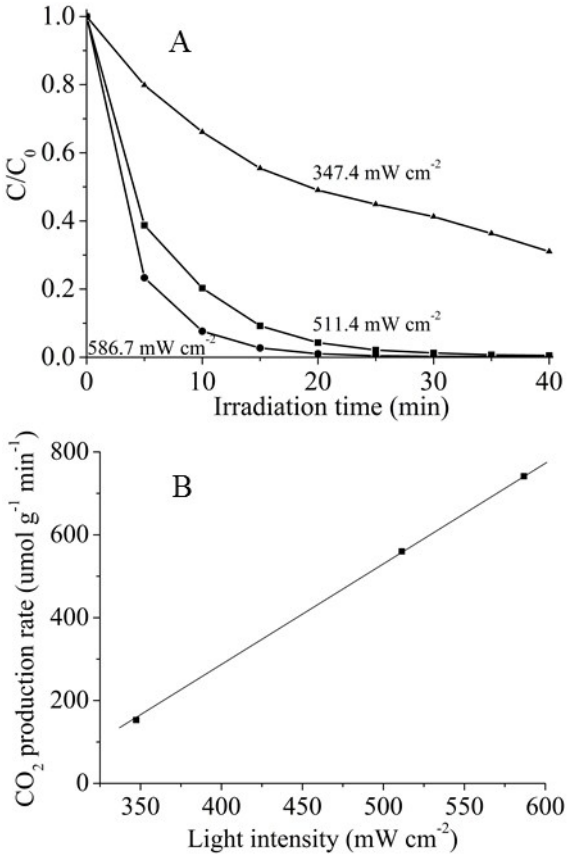

Figure S7. The time evolution of benzene concentration (A) and the initial CO_2 production rate of Co_3O_4-MNR for benzene oxidation of under the UV-Vis-IR illumination with different light intensity.

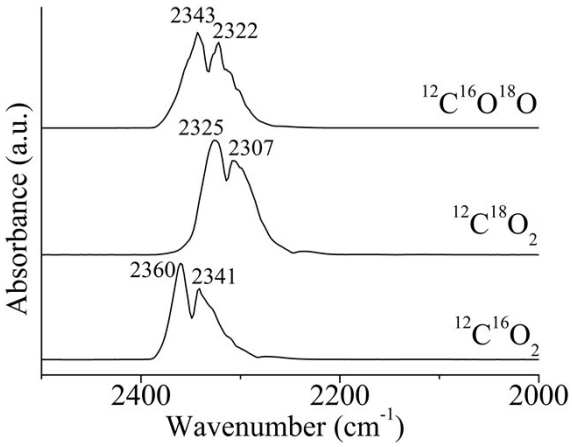

Figure S8. FTIR spectra of pure gases of $^{12}C^{16}O_2$, $^{12}C^{18}O_2$, and $^{12}C^{16}O^{18}O$ prepared by the oxidation of $^{12}C^{16}O$ by $^{18}O_2$ on 1.0 wt% Pt/Al_2O_3.

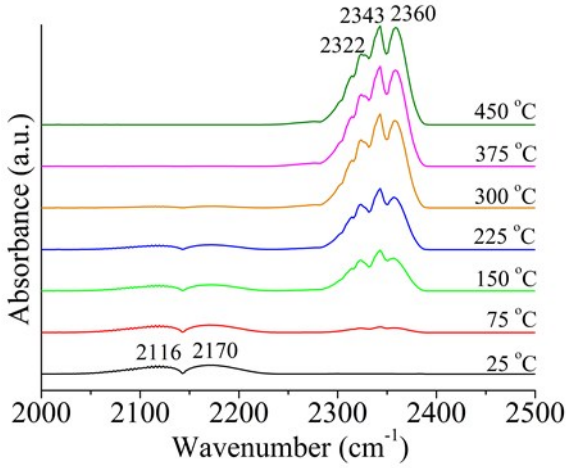

Figure S9. The evolution of FTIR spectra of the reactants and products for the used Co_3O_4-MNR sample (after the oxidation of benzene by $^{18}O_2$ on the fresh Co_3O_4-MNR sample under the UV-Vis-IR illumination for 70 min) in an atmosphere of $^{12}C^{16}O$ and N_2 at elevated temperatures. As shown in Figure S9, when the temperature increases to 150 °C, the strong double peaks of $^{12}C^{16}O^{18}O$ at 2343 and 2322 cm^{-1} are observed. This observation indicates that a considerable amount of ^{18}O exist in the used Co_3O_4-MNR sample and participate in the oxidation of $^{12}C^{16}O$. The strong peak of $^{12}C^{16}O_2$ at 2360 cm^{-1} (*note*: the peak at 2341 cm^{-1} of $^{12}C^{16}O_2$ overlaps with the peak at 2343 cm^{-1} of $^{12}C^{16}O^{18}O$) is observed. This observation indicate that a considerable amount of ^{16}O also exist in the used Co_3O_4-MNR sample and participate in the oxidation of $^{12}C^{16}O$. When the temperature increases to 225 and 300 °C, the peaks of both $^{12}C^{16}O^{18}O$ and $^{12}C^{16}O_2$ are significantly intensified, suggesting that more lattice oxygens of ^{16}O and ^{18}O in the used Co_3O_4-MNR sample participate in the oxidation of $^{12}C^{16}O$. When the temperature further increases to 375 and 450 °C, the peak intensity of $^{12}C^{16}O^{18}O$ at 2322 cm^{-1} almost remains unchanged, while the peak of $^{12}C^{16}O_2$ at 2360 cm^{-1} is obviously intensified. This observation indicates that the lattice ^{18}O in the used Co_3O_4-MNR sample is completely exhausted, and the bulk lattice ^{16}O in the used Co_3O_4-MNR sample migrates to the surface and participates in the oxidation of $^{12}C^{16}O$.

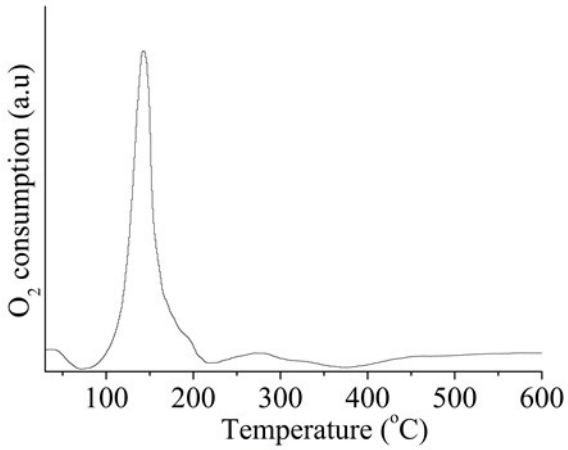

Figure S10. O_2-temperature programmed oxidation of the Co_3O_4-MNR sample pre-reduced by CO at 250 °C**.**